Optical and Thermal Assessment of a Linear Fresnel Collector Using a Minichannel Absorber Tube for Medium Temperature Applications

Pablo Castillo[1], Camila Correa[1], Ignacio Calderón[1], José Miguel Cardemil[1], Williams Calderón[1] and Gerardo Diaz[2]

[1] Mechanical Engineering Department, Universidad de Chile, Santiago (Chile)

[2] Department of Mechanical Engineering, University of California Merced, California (United States)

Summary

Solar thermal energy has been the fastest-growing renewable heat technology, but most of the world's solar thermal installed capacity consists of a single house domestic system. Linear Fresnel collectors are considered a cost-effective technology for applications such as heat for industrial process, concentrating solar power, etc. In 2008, Diaz presented a novel mini-channel tube solar collector for low temperatures applications, showing promising results compared to conventional flat plate and evacuated tube collectors. Considering the benefits of using mini-channels, the present work presents a novel design of a LFC by using a mini-channel tube as absorber. The main results show an increase of 2,8% of thermal power output and 21% in optical efficiency compared to commercial LFC, proving that this design could constitute a feasible option to be integrated into solar solutions for medium temperature industrial processes.

Keywords: Linear Fresnel, mini-channel tube, medium temperature, direct steam generation

1. Introduction

During 2017, renewable energies presented a total growth of 49% in the global energy matrix. Within these technologies, solar heat only represents 6.9% of installed capacity of renewable heat in domestic, commercial and industrial applications worldwide. Most of the solar thermal capacity consists of small domestic systems for single-family homes (IEA, 2017). Therefore, there is a vast potential for integrating solar heat for industrial processes, especially in regions where heat demand is growing due to the presence of industrial activity, such as food, agriculture, and chemicals. For this reason, it is of interest to study and develop solar thermal technologies, particularly for industrial applications.

Solar collectors are thermal components which act as heat exchangers, transforming solar radiation into useful heat by raising the temperature of a working fluid. Many industrial sectors require hot water at high temperatures or even steam for their processes, therefore concentrating solar collectors represent a promising technology for such applications. Linear Fresnel Collectors (LFC) are a type of line-focus concentrating collectors, which consist of a series of flat or slightly curved mirrors which track the sun during the day at different azimuth angles, reflecting solar radiation towards a fixed receiver, which depending on the absorber technology, can reach temperatures high enough for steam production. The advantage of their simple structural configuration, in terms of manufacture and installation, is usually concealed by the lower optical efficiency of LFC, due to their distorted focal line, compared to other concentrating solar technologies such as Parabolic Through Collectors (IRENA, 2012).

In 2001, the Belgian company Solarmundo developed a novel LFC prototype, claiming to be more cost-effective than existing concentrating technologies, because of its simpler tracking system, inexpensive flat mirror, and fixed absorber tube. The Solarmundo LFC prototype showed an optical efficiency of 61% at normal incidence (Häberle, 2001). Regarding the thermal efficiency of LFC receivers, due to its complex geometry, it has been mostly studied through computational simulations or experimental tests. For instance, Facão and Oliveira (2011) analyzed a trapezoidal cavity receiver via ray-tracing and CFD simulations, highlighting the influence of the receiver's geometry on the thermal efficiency. According to the Solar Heat for Industrial Processes (SHIP) database, there are only 13 LFC plants of a total of 313 CSP plants installed worldwide (IEA, 2019).

doi:10.18086/swc.2019.12.01 Available at http://proceedings.ises.org

In an effort to increase the overall efficiency of solar collectors, in 2008 Diaz presented a novel design with minichannel tubes as solar absorbers (Diaz, 2008). A channel is classified as mini-channel when its hydraulic diameter lies between 200 μm and 3 mm (Kandlikar and Grande, 2003). A mini-channel tube consists of an extruded flat tube with several mini-channel ports along its cross-section, as shown in Figure 1b. The purpose of the mini-channels is to increase the heat transfer area of the working fluid and reduce the thermal resistance of the heat flow since no external fin is needed. Later, Sharma and Diaz (2011) showed that the thermal efficiency of the evacuated-tube mini-channel collector increases significantly when compared to experimental data from conventional evacuated-tube collectors. In the same year, the Finnish company Savosolar presented a full-aluminum direct-flow absorber solar collector model using Multi-Port Extruded mini-channel profiles. This design won the Intersolar AWARD in 2011 (Savosolar, 2011). Savosolar began product deliveries in June 2011 and has since delivered over 75,000 m^2 of collectors for applications such as district heating, heat for industrial processes, space and building heating and domestic hot water. Additionally, in 2014, Robles et al. (2014) presented the design, manufacturing, testing and numerical simulation of an aluminum flat plate mini-channel solar collector, showing an increase in thermal efficiency of 13% compared to flat-plate collectors. A year later, Duong (2015) studied the use of mini-channel flat plate collectors for industrial applications at medium temperature (100-120ºC), reporting a low performance in indirect steam generation. Indeed, only a steam fraction of 0.00024 was obtained (2.4 g/min of steam from a 9.8 L/min water flow) under this configuration. Currently, there is no commercial mini-channel-based collector capable of producing heat at medium temperatures.

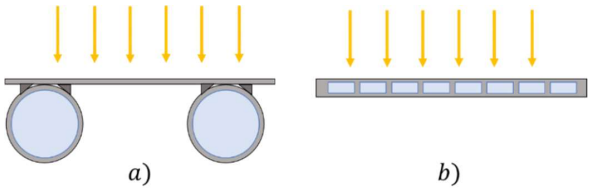

Figure 1. Sketch of: a) flat-plate collector, b) mini-channel tube collector. Dimensions not to scale.

Considering the reported advantages of using mini-channel collectors at low temperatures reported in the literature and the industry, this work presents a novel design of a LFC by using a mini-channel tube as an absorber, improving its performance for medium temperature applications (100-200ºC). The design process of the concentrator, receiver and mini-channel tube absorber is thoroughly described, and an optical and thermodynamic model is developed to fully evaluate the collector's performance in operational conditions. Both mathematical models were validated against commercial references and experimental data reported in the literature.

2. System description

A mini-channel-absorber LFC system is studied in this work. The main dimensions of this system are summarized as follows: The primary mirror field is 5.4 meters wide and 6 meters long. The mirror field consists of an array of 11 flat mirrors 40 cm wide and a trapezoidal cavity receiver with an internal copper mini-channel tube absorber, as shown in Figure 2. The trapezoidal cavity receiver with a base dimension of 440 mm, a base angle of 80º and a height of 120 mm is located at 3.9 meters above the mirror field. The mini-channel absorber tube is located at the top of the receiver and consists of a single flat tube with 128 rectangular ports. The dimension of each port is 2.5 mm wide by 2.0 mm height.

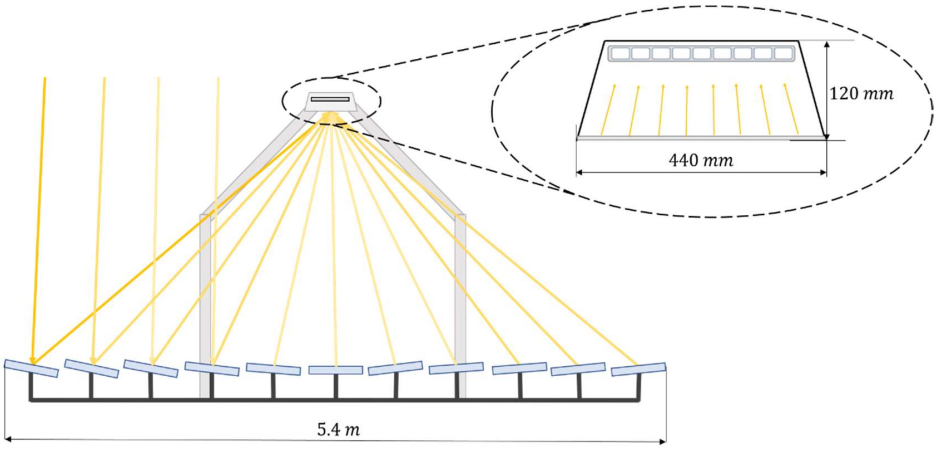

Figure 2. Sketch of the mini-channel linear Fresnel collector. Dimensions not to scale.

The geometric parameters of the collector are described in Table 1, and the optical and thermal properties are given in Table 2.

Table 1. Geometric parameters of the collector.

Parameter	Value
Number of primary mirrors	11
Width of the field	5.4 m
Width of the mirror	0.4 m
Length of the collector	6 m
Height of the receiver	3.9 m
Bottom width of the cavity	440 mm
Top width of the cavity	360 mm
Acceptance angle of the receiver	10º
Depth of the receiver	120 mm
Mini-channel tube width	360 mm
Mini-channel port width	2.5 mm
Mini-channel port height	2.0 mm
Number of ports	128

Table 2. Optical and thermal properties of the collector

Parameter	Value
Mirror reflectivity	0.95
Glass cover transmissivity	0.97
Glass cover reflectivity	0.08
Absorber coating absorptivity	0.95
Absorber coating emissivity	0.12
Copper thermal conductivity	400 W/(m K)

3. Mathematical Model

The optical and thermal processes in the linear Fresnel collector were modeled by a ray-tracing algorithm and a thermal resistance network, respectively. Both models are coupled at the base edge of the receiver. The details of the models are described in the following sections.

3.1. Optical model

The optical efficiency of a solar collector is a measure of the optical performance before considering the heat loss from the absorber to the environment. The optical efficiency of a concentrating collector is defined by the following equation (Duffie and Beckman, 2013):

$$\eta_{opt} = \rho(\gamma\,\tau\,\alpha)_n \cdot IAM \qquad \text{(eq. 1)}$$

where ρ is the specular reflectance of the concentrator, γ is the intercept factor defined as the fraction of the reflected radiation that is incident on the absorber, τ is the transmittance of any cover on the receiver, α is the absorptance of the absorber. The effect of the incidence angle on the previous parameters may be difficult to compute analytically. Thus, optical properties are calculated at normal incidence angle (0°) and an Incident

Angle Modifier (IAM) is defined to account the deviations from the real angle of incidence of the radiation.

The IAM reflects the non-symmetrical optical properties, which is a function of the transversal and longitudinal incidence angles, θ_T and θ_L respectively, therefore the optical efficiency at any incidence angle can be calculated as (Zhu, 2013):

$$\eta_{opt}(\theta_T, \theta_L) = \eta_{opt,0} \cdot IAM(\theta_T, \theta_L) \quad \text{(eq. 2)}$$

where $\eta_{opt,0}$ is the optical efficiency at normal incidence ($\theta_T = \theta_L = 0$). Assuming that the optical properties of the materials do not change with the incidence angle, the relationship between the intercept factor and IAM is given by:

$$IAM(\theta_T, \theta_L) = \gamma(\theta_T, \theta_L)/\gamma_0 \quad \text{(eq. 3)}$$

where γ_o is the intercept factor at a normal incidence. Finally, the IAM can be factorized into two independent functions of the transversal and longitudinal angle of incidence:

$$IAM(\theta_T, \theta_L) = K_T(\theta_T) \cdot K_L(\theta_L) \quad \text{(eq. 4)}$$

where K_T is the transversal incidence angle modifier and the longitudinal IAM is represented by K_L. The transversal IAM is computed by two-dimensional ray-tracing algorithm, which was developed considering the reflection, absorption, and transmission on every surface of the LFC, including the mirror field, trapezoidal receptor, and the mini-channel flat plate absorber. The ray-tracing algorithm calculates the nearest object that intercepts a ray path, then to compute the reflection process a uniformly distributed random number between 0 and 1 is generated, and according to the optical properties of the surface of the nearest object, the reflection process determines if the ray is reflected, absorbed or transmitted. This process is performed for every ray until it is absorbed or escapes the collector's transversal area. Then, the number of rays absorbed by absorber, in this case the mini-channel tubes, is computed and the intercept factor and transversal incidence angle modifier are calculated, as shown in the flowchart of the code in Figure 4.

To calculate the longitudinal angle modifier the following expression (Bellos and Tzivanidis, 2018) is utilized:

$$K_L(\theta_L) = \cos(\theta_L) - \frac{H}{L}\sin(\theta_L) \quad \text{(eq. 5)}$$

where H is the height of the receiver and L the length of the collector, as shown in Figure 3. Eq. 5 considers the cosine and non-illuminating losses in the longitudinal direction. Finally, the optical efficiency at any transversal or longitudinal angle of incidence can be calculated using eq. 1, eq. 4 and eq. 5.

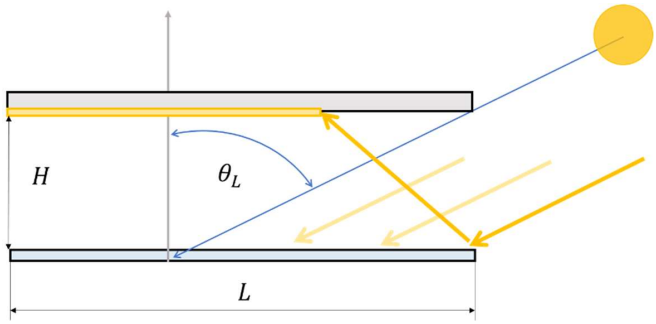

Figure 3. Sketch of the mini-channel LFC. Longitudinal view.

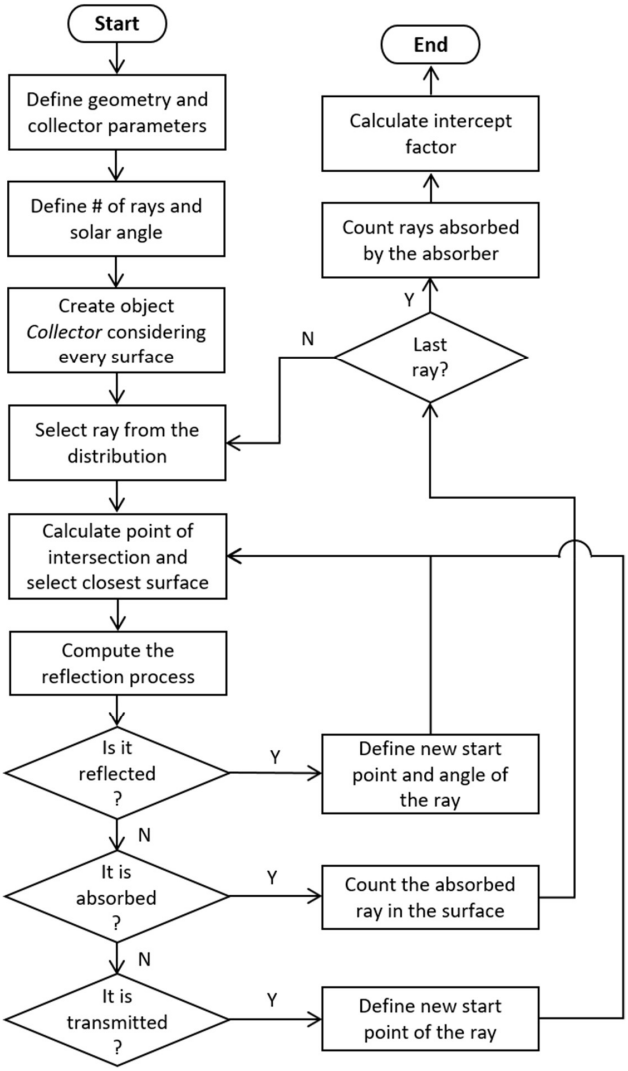

Figure 4. Flowchart of the 2D ray-tracing model to compute transversal IAM.

3.2. Thermal model

To analyze the thermal behavior of the absorber, a two-dimensional thermal model is proposed to represent the physical phenomena which occur within the receiver, as shown in Figure 5. This model considers single-phase flow (both liquid and vapor, separately) as well as two-phase flow, including the boiling process through the mini-channel's ports. The heat balances are based on the work of Robles et al. (2014) and Duong (2015), with modifications regarding the heat transfer assumptions on the heat conduction through the mini-channel and convective heat transfer correlation utilized. Both studies originally modeled the mini-channel as fin heat-exchangers, while the present work considers the heat transfer through the mini-channel as a constant surface temperature heat flows through four walls. This consideration induces significant modifications regarding the effect of boiling fluid through the channels.

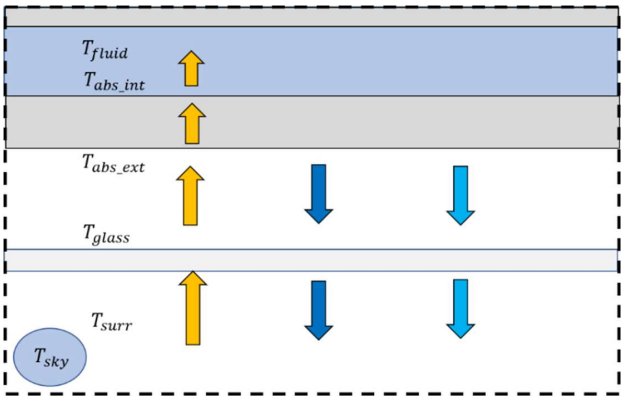

Figure 5. Energy transfer diagram through the receiver and mini-channel absorber.

Energy balances are performed in the collector's glass cover, absorber's inner and outer surface, and the working fluid. They are used to calculate the glass, absorber and fluid temperature through the collector length for a given mass flow rate and fluid inlet temperature. Due to the number of mini-channel's ports, transversal symmetry is assumed, then the energy balances are performed to only one port, considering the corresponding solar radiation and mass flow rate. These energy balances are presented for each relevant component in the following sections.

3.2.1. Glass cover

The energy balance for the glass cover is given by the following equation:

$$G_s + \left(\frac{\sigma}{\frac{1}{\epsilon_g} + \frac{1}{\epsilon_{abs} - 1}}\right)\left(T_{abs,ext}^4 - T_{glass}^4\right) + h_{air}\left(T_{abs,ext} - T_{glass}\right)$$

$$= h_{surr}\left(T_{glass} - T_{surr}\right) + \epsilon_g \sigma\left(T_{glass}^4 - T_{sky}^4\right) + \left(\frac{\alpha_{abs}\tau_g}{1-(1-\alpha_{abs})\rho_g}\right) G_s \qquad \text{(eq. 6)}$$

where G_s is the incident solar radiation, ϵ_g is the glass emissivity and ϵ_{abs} the emissivity of the absorber. The Stefan-Boltzmann constant is denoted by σ. $T_{abs,ext}$ is the external temperature of the absorber, T_{glass}, T_{surr} and T_{sky} are the temperatures of the glass cover, the surroundings, and the sky, respectively. The heat transfer coefficient h is defined for the air between the absorber and the glass cover (h_{air}) and for the heat transfer to the surroundings (h_{surr}). α_{abs} is the absorber absorptivity, τ_g and ρ_g are the glass cover transmissivity and reflectivity, respectively.

3.2.2. Absorber's inner and outer surface

An energy balance on the outer surface of the mini-channel absorber is carried out and it is defined by:

$$\left(\frac{\alpha_{abs}\tau_g}{1-(1-\alpha_{abs})\rho_g}\right) G_s = h_{air}\left(T_{abs,ext} - T_{glass}\right) + \varepsilon_g \sigma\left(T_{glass}^4 - T_{sky}^4\right) + \frac{\left(T_{abs,ext} - T_{abs,int}\right)}{R_{abs} P_{port} N_{port} L} \qquad \text{(eq. 7)}$$

where $T_{abs,int}$ is the internal temperature of the absorber and R_{abs} is the thermal resistance of the absorber and is determined by using the relation $R_{abs} = e_{mc}/(k_{cu} P_{port} N_{port} L)$. This is carried out under the assumption of a heat flux through the four walls of the mini-channel. Additionally, e_{mc} is the mini-channel thickness, k_{cu} the thermal conductivity of copper, P_{port} and N_{port} is the mini-channel perimeter and number of mini-channels, respectively. L is the length of the absorber.

On the other hand, at the inner surface of the absorber the heat transferred by conduction through the absorber and the heat transferred to the working fluid are considered, thus, the energy balance is given as follows.

$$\frac{T_{abs,ext} - T_{abs,int}}{R_{abs}} = h_f A_{int}\left(T_{abs,int} - T_{fluid}\right) \qquad \text{(eq. 8)}$$

where A_{int} is the internal area of the mini-channels, T_{fluid} is the fluid temperature and the heat transfer coefficient for single-phase fluids h_f.

3.2.3. Working fluid

The heat transferred to the fluid q_{fluid} produces an increase in enthalpy ΔH, that implies a rise of the fluid's temperature. The energy balance is given by:

$$h_f A_{int}\left(T_{abs,int} - T_{fluid}\right) = \dot{m} C_p \left(T_{fluid} - T_{in}\right) \quad \text{(eq. 9)}$$

where T_{in} is the inlet temperature of the collector with a mass flow $\dot{m}$. C_p is the heat capacity of the working fluid.

Equations (eq. 8) and (eq. 9) are defined for single-phase flows. Considering the case where the temperature of the working fluid is high enough to initiate the boiling process, the temperature of the fluid will remain constant, increasing the steam fraction. In this case, the correlation of Kandlikar and Balasubramanian, (2004) for two-phase heat transfer coefficient is utilized. Thus, the energy balance equations of the inner surface of the absorber and the working fluid, respectively, are defined as it follows, replacing equations 8 and 9:

$$\frac{T_{abs,ext} - T_{abs,int}}{R_{abs}} = h_{tp} A_{int} (T_{abs,int} - T_{fluid}) \quad \text{(eq. 10)}$$

$$h_{tp} A_{int}\left(T_{abs,int} - T_{fluid}\right) = \dot{m}\left\{\left(h_l + x(h_v - h_l)\right) - h_{in}\right\} \quad \text{(eq. 11)}$$

where h_{tp} is the heat transfer coefficient for two-phase flows, and the term $h_l + x(h_v - h_l)$ is the outlet enthalpy of the fluid, as a function of the enthalpy of the saturated liquid, saturated steam and the steam fraction, h_l, h_v and x respectively.

The thermal efficiency of the receiver is calculated with the following equation:

$$\eta_{th} = \frac{\dot{m}\{(h_l + x(h_v - h_l)) - h_{in}\}}{\left(\frac{\alpha_{abs}\tau_g}{1-(1-\alpha_{abs})\rho_g}\right) G_s A_{ext}} \quad \text{(eq. 12)}$$

where A_{ext} is the external area of the absorber. Finally, the useful thermal power output of the solar collector is calculated with the optical and thermal efficiency by the following equation.

$$\dot{Q}_u = \eta_{opt} \cdot \eta_{th} \cdot G_s \cdot A_m \quad \text{(eq. 13)}$$

4. Validation

A Python code was developed to compute the optical efficiency of the collector and the thermal energy balances on the receiver and mini-channel absorber. IAPWS library was utilized to determine the thermophysical properties of water and steam (IAPWS, 2018). To validate the results obtained with the developed two-dimensional ray-tracing algorithm, the Tonatiuh Monte-Carlo ray-tracing software (Blanco et al. 2005) was utilized to compute the transversal IAM of an evacuated tube LFC. The LFC consists of the same primary mirror array and trapezoidal cavity receiver presented in Section 2 but using a conventional evacuated tube absorber of 150 mm diameter. The same calculation procedure was performed by the two-dimensional ray-tracing algorithm. The results are shown in Figure 6. It is shown that the transversal IAM calculated by the two approaches are similar. The largest absolute error of the transversal IAM between Tonatiuh and two-dimensional ray-tracing is 0.036 (a relative error of 13%) in the case of an incidence angle of 80º.

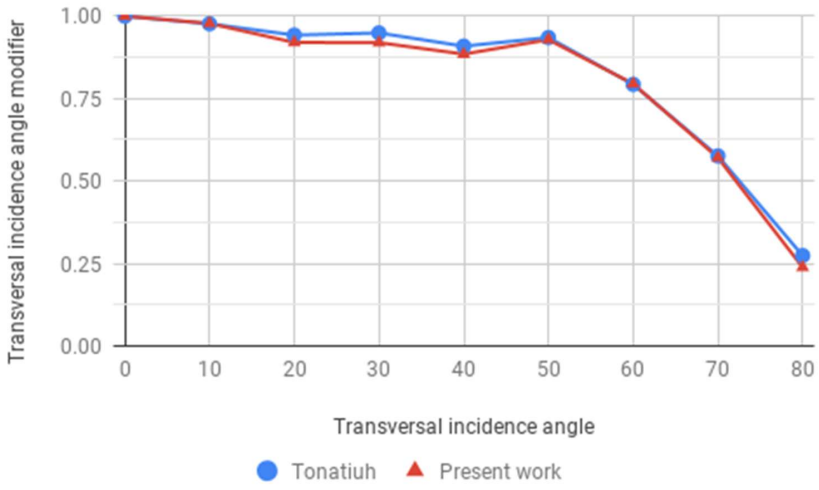

Figure 6. Transversal incidence angle modifiers for an evacuated tube linear Fresnel collector calculated with Tonatiuh and the present work.

To validate the thermal model, the thermal efficiency of a flat plate mini-channel collector was simulated at the same conditions as tested by Robles et al. (2014). The ambient temperature and global horizontal radiation was set to 20ºC and 900 W/m^2 respectively. The set of energy balances equations were solved using the bisection method implemented in Python. The thermal efficiency is plotted against $(T_{in} - T_{surr})/G_s$ in Figure 7, where a comparison between the model of Robles et al. (2014) and the present work is established. Good agreement is obtained between both models as the maximum absolute in thermal efficiency is only 0.013 or 1.25% in terms of relative error.

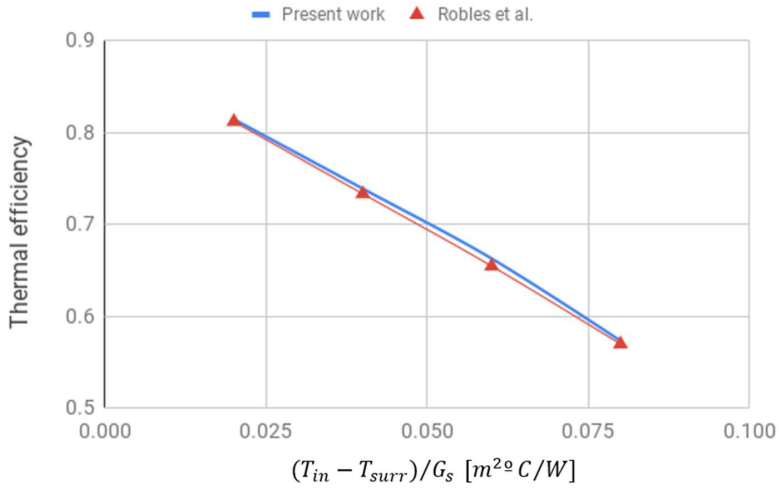

Figure 7. Comparison between mini-channel-based collector thermal efficiency of Robles et al. 2014, and the present work in terms of $(T_{in} - T_{surr})/G_s$.

5. Results

The performance of the mini-channel LFC is compared against a conventional LFC commercialized by Industrial Solar (Industrial Solar, 2011). The parameters used to compare these models under nominal conditions, such as ambient temperature, fluid inlet temperature, solar radiation and solar angles (zenith and

azimuth) are shown in Table 3.

Table 3. Nominal conditions parameters used to compare LFC performance.

Parameter	Value
Solar radiation (DNI)	900 W/m^2
Ambient temperature	30ºC
Fluid inlet temperature	160ºC
Azimuth angle	90º
Zenith angle	30º

The comparison of the thermal and optical performance under nominal conditions between both collectors is shown in Table 4. The proposed mini-channel LFC shows an increase of 2,8% of thermal power output by aperture area unit, reaching a value of 578 Wm^{-2}, compared to Industrial Solar LFC. Due to the larger absorption area and the receiver's geometry, the optical efficiency reaches a value of 0.773 which is over 21% more than in commercial LFC. However, as the mini-channel tube absorber is not evacuated, thermal losses are 7 times the reported in conventional LFC with evacuated tube absorbers.

Table 4. Performance characteristics of mini-channel linear Fresnel collector and commercial linear Fresnel collector.

	Presented work	Industrial Solar, 2011
Thermal output per aperture area unit	578 W/m^2	562 W/m^2
Thermal output per total installation area unit	471 W/m^2	377 W/m^2
Nominal optical efficiency	0.773	0.635
Thermal losses per longitudinal unit	519 W/m	< 70 W/m

After the promising results under nominal conditions, optical and thermal efficiencies are assessed under operational conditions, considering the transversal and longitudinal incidence angles from 90º to 0º, mass flow rate from 250 to 1400 kg/h, inlet temperature from 30ºC to 300ºC and direct normal irradiance from 300 to 1100 W/m^2. Transversal and longitudinal IAM for different incidence angles are shown in Figure 8. Both modifiers show good agreement with the typical optical behavior of a linear Fresnel collector, showing the maximum value for the transversal IAM at an angle of 40º, when the shadow of the receiver is projected out of the mirror field, and a decreasing longitudinal IAM due to cosine losses.

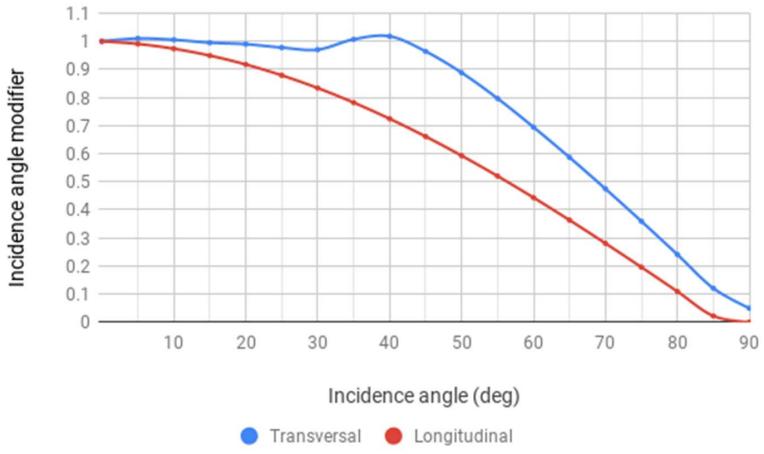

Figure 8. IAM as a factorized function of transversal and longitudinal incidence angles.

The effect of the mass flow rate and the DNI on the thermal efficiency of the mini-channel LFC is shown in Figure 9. A flat profile is obtained with any DNI when the mass flow rate is higher than 500 kg/h. This is due to the decrease in the outlet temperature and the thermal losses caused by the increase in the mass flow rate. Thus, higher flows do not generate a significant gain in thermal efficiency, while this is significantly affected by convective and radiative losses.

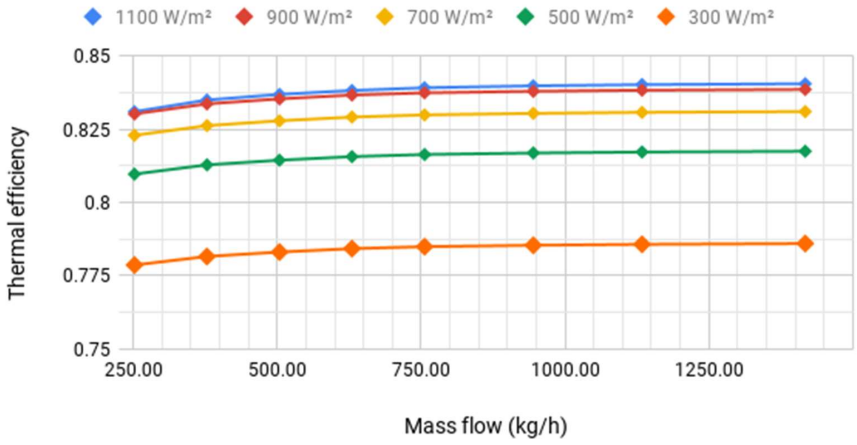

Figure 9. Effect of mass flow rate on efficiency of the mini-channel-based collector for different values of radiation.

For a given mass flow rate, Figure 10 shows the effect of the inlet temperature of the fluid on the thermal efficiency for different values of DNI. The thermal efficiency of the receiver decreases with the increase in the fluid inlet temperature mainly because of higher convective and radiative losses at such temperatures. However, for higher values of the DNI as 900 or 1100 W/m^2, thermal efficiency maintains a high value, close to 0.8, even for inlet temperatures of 300ºC, since the absorption of the solar radiation is higher than the thermal losses of the mini-channel tube absorber.

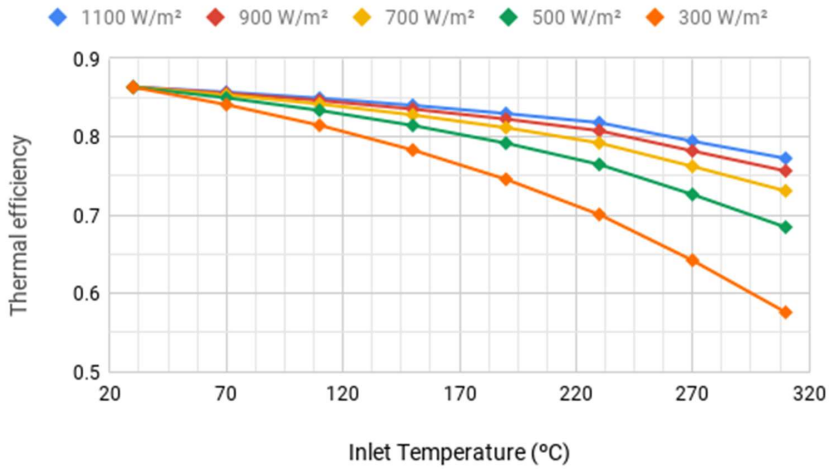

Figure 10. Effect of fluid inlet temperature on efficiency for different values of incident solar radiation.

6. Conclusions

The present work describes the assessment of a novel design of a linear Fresnel collector with a mini-channel tube absorber. The proposed configuration presents favorable results; showing an increase of 21% of optical efficiency over a conventional LFC. The performance of the collector is computed by numerical methods and compared to commercial LFC models. A two-dimensional ray-tracing model is developed to characterize the radiation's reflection in the mirror field, concentrator and the absorption in the mini-channel tube absorber. In addition, a thermal model was developed allowing to assess the heat transfer to the working fluid in single-phase operation and for medium temperature applications. The proposed collector presents only an increase of 2,8% of thermal power output by aperture area unit compared to commercial LFC, thus further improvements are necessary to reach higher efficiencies and thus a higher thermal output. Nonetheless, considering mini-channel tube absorbers could constitute a feasible option to facilitate the integration of solar technologies into medium temperature industrial processes. Future work is proposed to analyze the thermal model using CFD software; as well as experimental validation and annual energy production assessment of the proposed mini-channel linear Fresnel collector.

7. Acknowledgments

The authors appreciate the financial support from CONICYT/FONDAP 15110019 "Solar Energy Research Center" SERC-Chile, and the CONICYT REDI170176 project.

8. References

Bellos, E., Tzivanidis, C., 2018. Development of analytical expressions for the incident angle modifiers of a linear Fresnel reflector. Solar Energy 173, 769–779. https://doi.org/10.1016/j.solener.2018.08.019

Diaz, G., 2008. Performance Analysis and Design Optimization of a Mini-Channel Evacuated-Tube Solar Collector. Presented at the ASME 2008 International Mechanical Engineering Congress and Exposition, ASME, USA, pp. 61–67.

Duffie, J.A., Beckman, W.A., 2013. Solar Engineering of Thermal Processes 928.

Duong, V.T., 2015. Minichannel-tube solar thermal collectors for low to medium temperature applications. University of California, Merced, USA.

Facão, J., Oliveira, A.C., 2011. Numerical simulation of a trapezoidal cavity receiver for a linear Fresnel solar collector concentrator. Renewable Energy 36, 90–96. https://doi.org/10.1016/j.renene.2010.06.003

IAPWS, 2018. Revised Release on the IAPWS Formulation 2017 for the Thermodynamic Properties of Heavy Water.

IEA, 2019. Solar Thermal Plants Database | Solar Heat for Industrial Processes (SHIP) Plants Database [WWW Document]. URL http://ship-plants.info/solar-thermal-plants (accessed 8.8.19).

IEA, 2017. Tracking Clean Energy Progress 2017. OECD/IEA, Paris.

Industrial Solar, 2011. Technical Data. Industrial Solar linear Fresnel collector LF-11.

IRENA, 2012. Concentrating Solar Power, Renewable Energy Technologies: Cost Analysis Series. IRENA, United Arab Emirates.

Kandlikar, S.G., Balasubramanian, P., 2004. An Extension of the Flow Boiling Correlation to Transition, Laminar, and Deep Laminar Flows in Minichannels and Microchannels. Heat Transfer Engineering 25, 86–93. https://doi.org/10.1080/01457630490280425

Kandlikar, S.G., Grande, W.J., 2003. Evolution of Microchannel Flow Passages--Thermohydraulic Performance and Fabrication Technology. Heat Transfer Engineering 24, 3–17. https://doi.org/10.1080/01457630304040

Robles, A., Duong, V., Martin, A.J., Guadarrama, J.L., Diaz, G., 2014. Aluminum minichannel solar water heater performance under year-round weather conditions. Solar Energy 110, 356–364.

Savosolar, 2011. Savo-Solar Oy is Intersolar AWARD winner! [WWW Document]. Savosolar Oyj. URL https://savosolar.com/savo-solar-oy-is-intersolar-award-winner/ (accessed 8.8.19).

Sharma, N., Diaz, G., 2011. Performance model of a novel evacuated-tube solar collector based on minichannels. Solar Energy 85, 881–890.

Zhu, G., 2013. Development of an analytical optical method for linear Fresnel collectors. Solar Energy 94, 240–252. https://doi.org/10.1016/j.solener.2013.05.003